engineering proceedings

MDPI

Proceeding Paper

New Photoacoustic Cell Design for Solid Samples †

Judith Falkhofen [1,2,*], Bernd Baumann [1] and Marcus Wolff [1]

[1] Heinrich Blasius Institute of Physical Technologies, Hamburg University of Applied Sciences, Hamburg, Germany; email1@email.com (B.B.); email2@email.com (M.W.)
[2] School of Computing, Engineering and Physical Sciences, University of the West of Scotland, Scotland, UK
* Correspondence: judith.falkhofen@haw-hamburg.de
† Presented at the 10th International Electronic Conference on Sensors and Applications (ECSA-10), 15–30 November 2023; Available online: https://ecsa-10.sciforum.net/.

Abstract: We develop a new design of a photoacoustic (PA) cell particularly suited for quartz enhanced photoacoustic spectroscopy (QEPAS), where a quartz tuning fork (QTF) is used as a sound detector for the PA signal. The cell is designed for the investigation of solid and semi-solid samples and represents a unilateral open cylinder. The antinode of the sound pressure of the fundamental longitudinal mode of the half-open cylinder occurs directly at the sample, where a measurement is difficult. Therefore, the first harmonic is used. A small hole in the resonator wall at the location of the pressure antinode allows signal detection outside the cylinder without (or only minimally) changing the resonance conditions. This design is particularly simple and easy to manufacture. A finite element (FE) simulation is applied to determine the optimal cell length for the given frequency and the location of the pressure maximum. One difficulty is that the open end dramatically changes the acoustic sound field. We answer the research questions: Where is the sound pressure maximum located and do simple analytical equations agree with the results of the FE simulation?

Keywords: photoacoustic spectroscopy; QEPAS; solid samples; higher harmonics; resonator design; FE simulation;

1. Introduction

In photoacoustic spectroscopy, a sound pressure wave is generated by modulated laser radiation. The molecules absorb the light energy by converting it into bending and stretching oscillations and rotations or electronic transitions. The associated temperature variation is pulsating due to the modulated excitation, which leads to the development of sound waves. Over a wide range, the sound pressure amplitude is proportional to the concentration of the molecules under investigation. In contrast to gaseous samples, where the photoacoustic signal is often generated over the length of the laser beam within the cell, the signal of solid samples is generated directly at the surface of the sample or even slightly below [1,2].

Often, acoustic resonances of the sample cell are exploited to improve the signal-to-noise ratio (SNR) of the PAS measurement. Special cells have been developed for the photoacoustic investigation of solid samples, e.g., in a cuboid [3,4] or a T shape [5,6]. The latter was also modelled using Finite Element Methods (FEM) and optimised concerning the signal amplitude [7].

Recently, quartz tuning forks (QTF) with resonance frequencies beginning in the kHz region are used to detect the acoustic signal. QTFs possess a high specificity for separating noise in other frequency ranges from the signal. More advantages are high frequency stability over a wide temperature range, insensitivity to magnetic fields and a high resonance quality factor. Low costs and small size make them suitable for small sensors in mass production [8–10].

Citation: Falkhofen, J.; Baumann, B.; Wolff, M. New Photoacoustic Cell Design for Solid Samples. **2023**, *56*, x. https://doi.org/10.3390/xxxxx

Academic Editor(s): Name

Published: 15 November 2023

In this article we present the design of a half-open cylindrical resonator for the photoacoustic investigation of solid samples particularly suited for QEPAS. One end of the tube is tightly sealed by the sample. The laser beam enters at the opening on the other side. The cell is considerably simpler to manufacture than a cuboid or T shaped cell. The T cell consists of two different cylinders, coupled together. Often the larger one is referred to as cavity cylinder and the one leading to the acoustic sensor as resonance cylinder. The sample is attached to the cavity cylinder and the sound generated there has to couple into the second, geometrically much narrower resonance cylinder which is accompanied by an additional damping because impedance discontinuities between large and small pipes usually lead to considerable energy losses [11]. It is expected that the signal of the new cell will be significantly higher compared to the T cell.

The following section shortly comprises the theoretical background of sound propagation in a resonant cell in the case of the PA signal of a solid sample. Chapter 3 describes the finite element (FE) model and the results of the simulation. Chapter 4 contains a discussion and an outlook.

2. Acoustically Resonant PA Cell

PAS experiments with solid samples were already carried out by Alexander Bell [12]. The absorption spectrum of solid samples can be observed more easily with PAS than with conventional spectroscopy techniques since scattered light plays for the PA signal no important role. The primary source of the PA signal is the result of periodic heat flow from the solid to the surrounding gas [13].

The SNR of the PA signal is intended to be enlarged by the resonator described here. In the cylinder a standing wave is developing due to reflections at the tube's ends and the superposition of the waves. If the radius a of the tube is much smaller than the wavelength, the acoustic wave is basically longitudinal. At open ends the sound wave does not undergo a phase shift, whereas closed ends lead to a phase shift of 180 degrees. In this application of a half-open cylinder the tube will be in resonance if its length l' and the frequency f_m are connected by the equation [14]

$$f_m = \frac{(2m-1)c}{4l'}, \quad m = 1, 2, 3 \ldots \tag{1}$$

Here, $l' = l + \Delta l$, where l is the geometric length of the cylinder and Δl is called end correction. At the open end, it can be assumed that the reflection takes place at an imaginary point Δl away from the plane defined by the open cylinder end. The end correction is an effect resulting from a mismatch between the essentially one-dimensional acoustic field inside the pipe and the three-dimensional field radiated by its open end [14]. The corrected overall length l' is also called the effective length of the cylinder. The end correction can be calculated from [15]

$$\Delta l = 0.6133 \cdot a. \tag{2}$$

Due to loss effects the true resonance frequencies are slightly lower than the eigenfrequencies. Therefore, the real end correction is slightly larger than the calculated value according to Equation (2). In order to obtain the highest possible photoacoustic signal, the radiation should be modulated with a frequency corresponding to the most intense acoustic resonance. Since the intensity decreases with increasing mode order [16] and the fundamental longitudinal resonance leads to a sound pressure maximum directly at the sample, the first harmonic of the longitudinal resonance is used. The according sound pressure distribution is schematically shown in Figure 1.

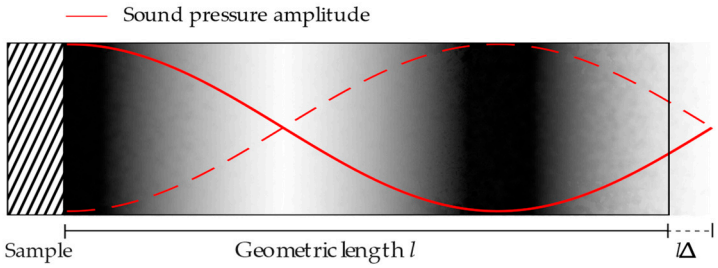

Figure 1. Sound pressure distribution of the first harmonic longitudinal resonance of a half-open cylinder.

In upcoming experiments, a commercial quartz tuning fork will serve as sound detector for the photoacoustic signal [17]. Its resonance frequency is $f_R = 32.768$ kHz. The placement of the tuning fork in the so-called off-beam configuration is shown in Figure 2.

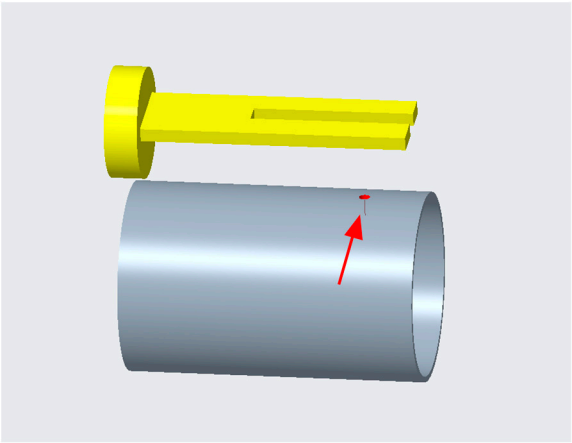

Figure 2. Cell with hole (marked with arrow) in a QEPAS off-beam configuration.

Since the sample is stimulated by a laser beam, the diameter of the cylinder has to be larger than the beam width. The laser beam must not hit the wall of the tube. Otherwise, this results in a wall signal that interferes with the wanted PA signal of the sample. In this investigation the radius of the tube is

$$a = 2 \text{ mm}. \tag{3}$$

Combining the end correction formula Equation (2) with the resonance frequency of the first harmonic f_2 matching the QTF resonance frequency f_R, leads to a geometric length of the pipe

$$l = 6.6240 \text{ mm}, \tag{1}$$

where for the speed of sound the value $343\ {}^{\text{m}}/_{\text{s}}$ has been used.

3. Finite Element Simulation

To obtain an independent and presumably more accurate result for l, we performed a simulation using the FE tool COMSOL Multiphysics®. Also, we aimed to get information on the location of the maximum of the sound pressure.

The simulation numerically solves the homogenous Helmholtz equation

$$\nabla^2 p(\vec{r}) + k^2 p(\vec{r}) = 0 \tag{5}$$

for the acoustic pressure field $p(\vec{r})$ with the wave number k. At the sound hard walls (the cylinder walls, the closed end and a plane surface defined by the flange at the

resonator's open end) the boundary condition applies. The normal derivative of the pressure is zero at the boundary.

$$\frac{\partial p}{\partial n} = 0 \tag{6}$$

For the Helmholtz Equation the truncation of a simulation domain for the open cylinder end is non-trivial. Conventional or periodic boundary conditions generate artifacts. A well-established method to deal with this problem is to define a perfectly matched layer (PML). PMLs can be imagined as non-reflecting wave absorbers [18].

The solutions of the differential Equation (5) subject to the described boundary conditions comprise the modes $p_m(\vec{r})$ and the corresponding value k_m. The eigenfrequencies are given by

$$\omega_m = ck_m, \tag{7}$$

where c is the velocity of sound [19]. It is assumed that the sample is sound hard, closes the tube soundproof and that vibrations of the resonator walls are negligible.

To determine the geometric length of the tube and the location of the antinode of the sound pressure near the open end of the cylinder, a 2D axially symmetric FE model is used. Initially, l is set to the estimate of Equation 4. Then the cylinder length is gradually varied until the eigenfrequency matches with the resonance frequency of the QTF (trial and error). The result of this procedure is

$$l_{FE} = 6.6605 \text{ mm} \tag{8}$$

In comparison to the analytical result (Equation (4)) the result of the FE simulation is 0.55% (0.037 mm) higher. The difference of the two methods is remarkably small. The FEM is supposed to rely on less approximations and is therefore considered more accurate.

Figure 3a shows the resulting sound pressure distribution of the first harmonic longitudinal mode in the centre plane of the cylinder closed by the sound-hard sample at the lower end. The semi-circle shaped domain attached to the upper end of the resonator represents the outer space. The PML is implemented in the semi annulus. In Figure 3b the FE mesh used for the simulations is depicted. The mesh is the result of a convergence study. The number of degrees of freedom is approximately 4500.

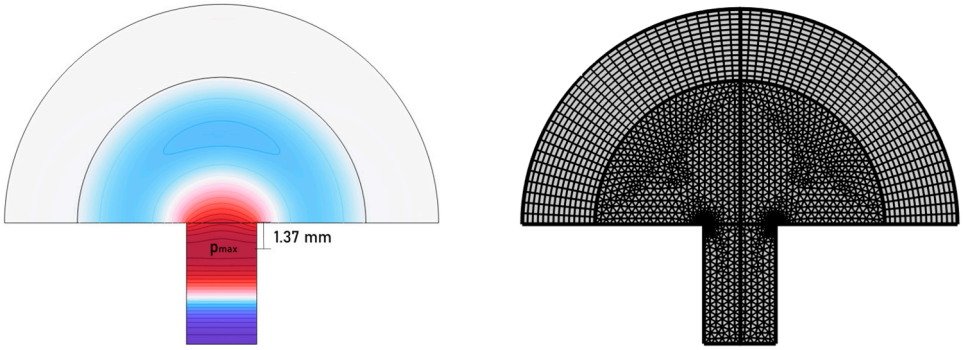

(a) (b)

Figure 3. (**a**) Sound pressure distribution at the central plane of the new cell at $f_1 = 32.768$ kHz. Dark blue and dark red correspond to the highest pressure values, which are 180 degrees out of phase. The distance of the maximum sound pressure to the open end is marked. (**b**) FE mesh. The PML is defined on the outer semi annulus.

As expected, the sound pressure of the mode spreads into the exterior space. The sound pressure maximum is located 1.37 mm from the open end. This is supposed to be

the optimal location for the sound detector. In order to avoid a substantial distortion of the sound field, a small hole could be drilled and the QTF placed in front of it (see Figure 2).

4. Discussion and Outlook

A simple cylindrical cell design of a PAS cell for measurements with QEPAS and solid samples has been developed. For the first harmonic longitudinal resonance the results for the end correction of an analytical estimate and a numerical calculation are similar. It is expected that the properties of the QTF can optimally complement the resonance behaviour of the small cylinder. The simple and inexpensive sensor design is also suitable for a miniaturised mass product. Since the expectation for the signal is that the SNR is larger than that of a T shaped cell, these will be compared in the following experimental test series.

The next step will be to consider the effect of the drilling on the sound pressure field inside the tube. In the experimental testing of the sensor, it is planned to investigate the dependency of the PA signal on the distance between the sound detector and the outer tube wall. Furthermore, the sample attachment can be examined more closely. Since the signal is generated at the surface of the sample, it is essential that it has a flat and smooth surface and is aligned perpendicular and acoustically sealed to the cylinder end.

Author Contributions: Conceptualization, M.W.; methodology, B.B., J.F.; software, B.B.; writing—original draft preparation, J.F., B.B.; writing—review and editing, J.F., B.B. and M.W.; visualization, J.F.; supervision, M.W. All authors have read and agreed to the published version of the manuscript.

Funding: This research received no external funding.

Data Availability Statement: No further than the shown new data were created or analyzed in this study. Data sharing is not applicable to this article.

Acknowledgments: We would like to thank the 3D printing teams of the Hamburg University of Applied Sciences for the friendly support and the company MeKo for the good cooperation in creating the small cylinders.

Conflicts of Interest: The authors declare no conflict of interest.

References

1. Friedrich, C.S. Photoakustik mit Halbleiterlasern. *Cuvillier Verl. Göttingen* **2012**.
2. Sarode, A.; Mahajan, O. Theoretical aspects of Photoacoustic Signal Generation with Solid Crystals. *Bull. Karaganda Univ. Phys. Ser.* **2021**, *104*, 61–67, https://doi.org/10.31489/2021ph4/61-67.
3. Raghu, O.; Philip, J. A dual channel photoacoustic cell for imaging experiments on solid samples. *J. Instrum. Soc. India* **2003**, *33*, 155–158.
4. Rabasović, M.D.; Nikolić, M.G.; Dramićanin, M.D.; Franko, M.; Markushev, D.D. Low-cost, portable photoacoustic setup for solid samples. *Meas. Sci. Technol.* **2009**, *20*, 095902. https://doi.org/10.1088/0957-0233/20/9/095902.
5. El-Busaidy, S.; Baumann, B.; Wolff, M.; Duggen, L.; Bruhns, H. Experimental and Numerical Investigation of a Photoacoustic Resonator for Solid Samples: Towards a Non-Invasive Glucose Sensor. *Sensors* **2019**, *19*, 2889. https://doi.org/10.3390/s19132889.
6. El-Busaidy, S.A.S.; Baumann, B.; Wolff, M.; Duggen, L. Modelling of open photoacoustic resonators. *Photoacoustics* **2020**, *18*, 100161. https://doi.org/10.1016/j.pacs.2020.100161.
7. El-Busaidy, S.; Baumann, B.; Wolff, M.; Duggen, L. Shape Optimization of an Open Photoacoustic Resonator. *Appl. Sci.* **2021**, *11*, 2571. https://doi.org/10.3390/app11062571.
8. Patimisco, P.; Sampaolo, A.; Zheng, H.; Dong, L.; Tittel, F.K.; Spagnolo, V. Quartz–enhanced photoacoustic spectrophones exploiting custom tuning forks: a review. *Adv. Physics X* **2017**, *2*, 169–187. https://doi.org/10.1080/23746149.2016.1271285.
9. Zifarelli, A.; Menduni, G.; Giglio, M.; Sampaolo, A.; Patimisco, P.; Wu, H.; Dong, L.; Spagnolo, V. Latest Advances in Quartz Enhanced Photoacoustics Spectroscopy for Environmental and Industrial Ap-plications. In Proceedings of the 23rd International Conference on Transparent Optical Networks (ICTON), Bucharest, Romania, 2–6 July 2023; pp. 1–3.
10. Ayache, D.; Rousseau, R.; Kniazeva, E.; Charensol, J.; Seoudi, T.; Bahriz, M.; Gouzi, F.; Spagnolo, V.; Vicet, A. Commercial and Custom Quartz Tuning Forks for Quartz Enhanced Photoacoustic Spectroscopy: Stability under Humidity Variation. *Sensors* **2023**, *23*, 3135. https://doi.org/10.3390/s23063135.
11. Peat, K. The acoustical impedance at discontinuities of ducts in the presence of a mean flow. *J. Sound Vib.* **1988**, *127*, 123–132. https://doi.org/10.1016/0022-460x(88)90353-7.

12. Manohar, S.; Razansky, D. Photoacoustics: a historical review. *Adv. Opt. Photon* **2016**, *8*, 586–617. https://doi.org/10.1364/aop.8.000586.
13. Rosencwaig, A.; Gersho, A. Theory of the photoacoustic effect with solids. *J. Appl. Phys.* **1976**, *47*, 64–69. https://doi.org/10.1063/1.322296.
14. Miklós, A.; Hess, P.; Bozóki, Z. Application of acoustic resonators in photoacoustic trace gas analysis and metrology. *Rev. Sci. Instrum.* **2001**, *72*, 1937–1955. https://doi.org/10.1063/1.1353198.
15. Levine, H.; Schwinger, J. On the Radiation of Sound from an Unflanged Circular Pipe. *Phys. Rev. B* **1948**, *73*, 383–406. https://doi.org/10.1103/physrev.73.383.
16. Wu, D.; Gao, S.; Li, J.; Yao, L.; Yu, X.; Zhang, Z.; Zhang, H.; Wang, X. Amplitude and phase relation of harmonics in nonlinear focused ultrasound. *AIP Adv.* **2022**, *12*, 065317. https://doi.org/10.1063/5.0096071.
17. Ma, Y. Review of Recent Advances in QEPAS-Based Trace Gas Sensing. *Appl. Sci.* **2018**, *8*, 1822. https://doi.org/10.3390/app8101822.
18. Johnson, S.G. Notes on perfectly matched layers (PMLs). *arXiv* **2021**, arXiv:2108.05348.
19. Baumann, B.; Wolff, M.; Kost, B.; Groninga, H. Finite element calculation of photoacoustic signals.. *Appl. Opt.* **2007**, *46*, 1120–1125. https://doi.org/10.1364/ao.46.001120.